Journal of Natural Gas Science and Engineering 70 (2019) 102967

Contents lists available at ScienceDirect

Journal of Natural Gas Science and Engineering

journal homepage: www.elsevier.com/locate/jngse

Wetted wall fraction of gas-liquid stratified co-current two-phase flow in a horizontal pipe with low liquid loading

Deendarlianto[a,b,*], Akhmad Zidni Hudaya[a,c], Indarto[a,b], Katya Dara Ozzilenda Soegiharto[b]

[a] Department of Mechanical and Industrial Engineering, Faculty of Engineering, Universitas Gadjah Mada, Jalan Grafika 2, Yogyakarta, 55281, Indonesia
[b] Center for Energy Studies, Gadjah Mada University, Sekip K-1A Kampus UGM, Yogyakarta, 55281, Indonesia
[c] Department of Mechanical Engineering, Universitas Muria Kudus, Kampus Gondangmanis, Kudus, Central Java, Indonesia

ARTICLE INFO

Keywords:
Stratified flow
Wetted wall fraction
Contact angle
Circumferential liquid film thickness

ABSTRACT

An investigation of the wetted wall fraction of gas-liquid stratified co-current two-phase flow in a horizontal pipe with low liquid loading was carried-out experimentally. The pipe length and the inner pipe diameter were 10 m and 26 mm respectively. The tested fluids were air and water. The superficial water (J_L) and air (J_G) velocities ranged from (0.02–0.075) m/s and (4–16) m/s respectively. In the experiments, the circumferential liquid film thickness was measured by using developed parallel wire sensor, and verified by the analyzed image of the axial view of the visual observations. At the same time, the pressure gradient and liquid hold-up data were taken in order to determine the interfacial shear stress between gas and liquid. The results indicate that (1) J_L and J_G significantly affect the interfacial shape of gas and liquid stratified flow in a horizontal pipe, whereas starting from $J_G = 8$ m/s the interfacial shape changes from flat-shaped to concave-shaped interfaces, (2) a new correlation to predict the wetted wall fraction (WWF) of gas-liquid stratified flow in a horizontal pipe was also proposed, and yielded the mean absolute prediction error (MAPE) of 20.6% in comparison with the obtained experimental data from the present study and the available data in open literatures.

1. Introduction

Gas-liquid co-current stratified two-phase flow under the condition of low-liquid-loading is the simplest flow pattern among the two-phase flow patterns inside the horizontal pipe during the hydrocarbon transportation from the oil well to the refinery plant under steady or transient conditions. Here low-liquid-loading is defined as a flow condition where the ratio of the liquid flow rate to gas flow rate is very small (Vuong et al., 2018), or in the form of the value of the liquid hold is approximately 0.30. In the practical application, the stratified flow also has an advantage due to its stability and ease of the separation of liquid and gas. It is characterized by a separation of the liquid and gas phases due to the difference of density. Here the small waves are formed at the interface of gas and liquid if the gas or the liquid rate is increased, in which the interfacial film is affected by both the surface tension and liquid viscosity. Moreover Vuong et al. (2018) also reported that the stratified two-phase flow is more complex than the single phase flow due to the slippage between gas and liquid that results in the change of distribution of the phases in the pipe, and it affects the performance of the transportation pipeline. Therefore the understanding of such flow characteristics is very important to ensure the safe operations of the hydrocarbon transportation pipelines and their downstream facilities.

Ullmann and Brauner (2006) noted that the existence of the interfacial wave during a stratified flow increases the drag between the phases, therefore, causing a considerable pressure gradient increment. In general, to predict those pressure gradients, solving the equations in the one-dimensional (1-D) two-fluids model is needed, which are dependent on the available data or experimental correlation of wetted wall fraction (WWF). In fact, the shape of the interface is somehow unknown. In the present study, the WWF is defined as the ratio of the wetted perimeter by the liquid phase to the total perimeter of the circumferential pipe wall as suggested by Ahn et al. (2018), and is related to interfacial transfer terms in the two-fluid model. Furthermore, Ayati et al. (2014) noted that the complexity of the underlying physics during the interaction between gas and liquid at the interface has not been understood well. For instance, the interfacial shear stress of a gas-liquid stratified flow could not be predicted well due the unavailability of the WWF information. Moreover, it is important to accurately predict the interfacial shear stress to ensure an optimal operation and proper design of the flow, in which the circumferential liquid film thickness in a

* Corresponding author. Department of Mechanical and Industrial Engineering, Faculty of Engineering, Universitas Gadjah Mada, Jalan Grafika 2, Yogyakarta, 55281, Indonesia.
E-mail address: deendarlianto@ugm.ac.id (Deendarlianto).

https://doi.org/10.1016/j.jngse.2019.102967
Received 21 May 2019; Received in revised form 10 August 2019; Accepted 12 August 2019
Available online 14 August 2019
1875-5100/

horizontal pipe is larger in the bottom part than it is in the upper part due gravity. This will in turn affect the flow conditions of the gas and liquid, and consequently change the flow instability.

Experimental and numerical investigations on the WWF were carried out in the past. Taitel and Dukler (1976) used the assumption of a flat interface in the calculation of the wetted wall fraction to solve the one dimensional separated flow model under the condition of a steady state in a horizontal pipe. However the experimental investigation from Fukano and Ousaka (1989) reported that the liquid film spreads up along the circumference of the pipe wall due to the pumping action of the disturbing waves, therefore the interface of gas and liquid is expected to have a concave shape.

Hart et al. (1989) proposed a prediction of the WWF on the basis of the balance between the potential and partial kinetic energies under the low liquid loading. They assumed that the shape of the interface was a truncated ring, and found that the change of surface tension does not affect the value of WWF at low WWF region. Although the proposed model by Hart et al. is able to predict the WWF under low liquid loading, the assumption that the shape of interface is truncated and therefore has the identical circumferential liquid film thickness at any given angle was far from the real physique and was not supported by real experimental data. Therefore the development of an experimental correlation on the basis of the real physique of the interface from the real experimental data is needed.

In terms of the theoretical development on the wall and interfacial shear stress of a stratified flow in a horizontal pipe, Ullmann et al. (2004) derived theory-based closure relations for laminar stratified flows. Here, the interaction of phases were accounted. They reported that the model could predict the pressure gradient and hold-up for a wide range of dimensionless parameters in counter and co-current laminar stratified flows. However it was generally developed in liquid-liquid systems, therefore it may be irrelevant to the practical implementation of gas-liquid laminar two-phase flow. Moreover, Ullmann and Brauner (2006) developed new correlations of the concave interface based on the experimental data available from open literature on the basis of the mechanism of the secondary gas flow in stratified flow in horizontal channel. They claimed that the correlation fits well with the case of low liquid loading, in which the interfacial shape is a constant curved arc. Although the proposed correlation could correlate the experimental data, if it is applied to the momentum equations in two-fluid models, the result does not match the physical shape that it should. Because in this case, the curvatures are unchanged by such momentum equations. Moreover, the prediction in the region of the gas-liquid up-flow by using the correlation needs an extra careful approach due to the high sensitivity of the result and assumptions. Therefore more experimental data are needed in order to develop a high performance experimental correlation to predict the WWF of a gas-liquid stratified flow in horizontal pipes.

The aim of the present experimental work is to investigate the WWF during the transportation of a gas-liquid stratified flow in horizontal pipe over a wide range of superficial velocities of gas and liquid. In the present manuscript, the effect of the superficial velocities of gas and liquid on the shape of interface will be provided first. From those data, the transition flow pattern map of the shape of interface will be developed. Moreover the circumferential data of the liquid film thickness will be given, and finally a new semi empirical correlation of the WWF will be proposed.

2. Experimental apparatus and procedure

2.1. Description of flow loop

Fig. 1 shows the schematic diagram of the experimental apparatus used in the present experimental study. The detail of the apparatus and procedure were described clearly by Setyawan et al. (2016); Setyawan et al. (2017), Dinaryanto et al. (2017), Hudaya et al. (2019), Deendarlianto et al. (2019), and only the main features are presented here. The working fluids were air and water. The tested pipe was acrylic pipe. The inner pipe diameter and length of the tested pipe were 26 mm and 10 m respectively. The experiments were performed under the atmosphere condition.

A compressor with the maximum mass flow of 600 LPM and pressure of 8 bars (gauge) was used to obtain the desirable airflow rate. Here, an air valve was used to constantly control the pressure that flowed in. To control the airflow rate, three Dwyer gas rotameter with the maximum capacities of 200, 600, and 1600 SCFH were used, with approximately 3% of accuracy. The needed water supply was given by pumping water from a storage tank using a centrifugal pump with a maximum capacity of 16.8 m^3/hour. To measure the water flow, an Omega water rotameter with a maximum capacity of 75 GPH and approximate accuracy of 2% was used. Besides that, a flexible tube was installed with the purpose of minimising flow oscillation and vibration near the inlet area.

After all was set, air was compressed from the compressor to the air flow meter and mixed with the water inside a simple T-mixer at the same time. The detailed drawing of the air and water mixer can be found in Hudaya et al. (2019). Inside this mixer, a splitter plate with a thickness of 3 mm was placed to reduce the flow fluctuation during the formation of the stratified flow. After being mixed, the air and water then flow in together towards the test section. At the end of this section, a separator is installed. Here, air is released into the atmosphere and water is sent back to the storage tank before re-entering the inlet.

Experiments were conducted under atmospheric conditions. It was assumed that the system was not affected by the surroundings, therefore, no transfer of heat passed the system's boundaries. The water superficial velocity (JL) varied between 0,02 m/s and 0,075 m/s, and air superficial velocity was set between 4 m/s and 16 m/s.

2.2. Test section

The circumferential liquid film thicknesses of the stratified flow inside the tested pipe were measured by using developed two parallel wire sensors. The distance between the sensors was 215 mm representing the approximate distance of the liquid wave of the observed flow pattern. The sensor includes a pair of silver-plated copper wire with a diameter of 0.5 mm and the space between the wires was 5 mm as shown in Fig. 2 (a). The sensor was equipped with a voltage divider circuit (Fig. 2 (b)) with a 12 V DC voltage source as a signal conditioner. The signal output from the circuit was then sent to a personal computer via the amplifiers and an analog/digital converter.

The calibration of the measured circumferential liquid film thickness was carried out by comparing the measured output signal from the sensor in the form of voltage difference and the measured liquid film thickness using a micrometer at the beginning of each experimental run. Here the interpolation of piecewise Lagrange was used to change the voltage data into the liquid film thickness. Furthermore, the contact angles inside the pipe were investigated by rotating the parallel wire sensors with respect to the axis of the pipe to the corresponding angle as shown clearly in Fig. 2(a). Here the WWF was determined as the value of the rotation angle, in which the thickness of the film approached zero.

The measurements of the instantaneous liquid hold-up (η) inside the test pipe were performed using the constant electric current method (CECM) as shown in Fig. 3. The working principle of the CECM method uses the difference in the electric resistance between the gas and the liquid phases as explained by Fukano (1998). As shown in the Figure, we have used five sensors arranged with an axial spacing of 215 mm. The working principle of CECM is based on the difference of the electrical resistance of the liquid and gas. The resistance of the two-phase flow, $R_{TP,}$ in the unit of pipe length is expressed as follows:

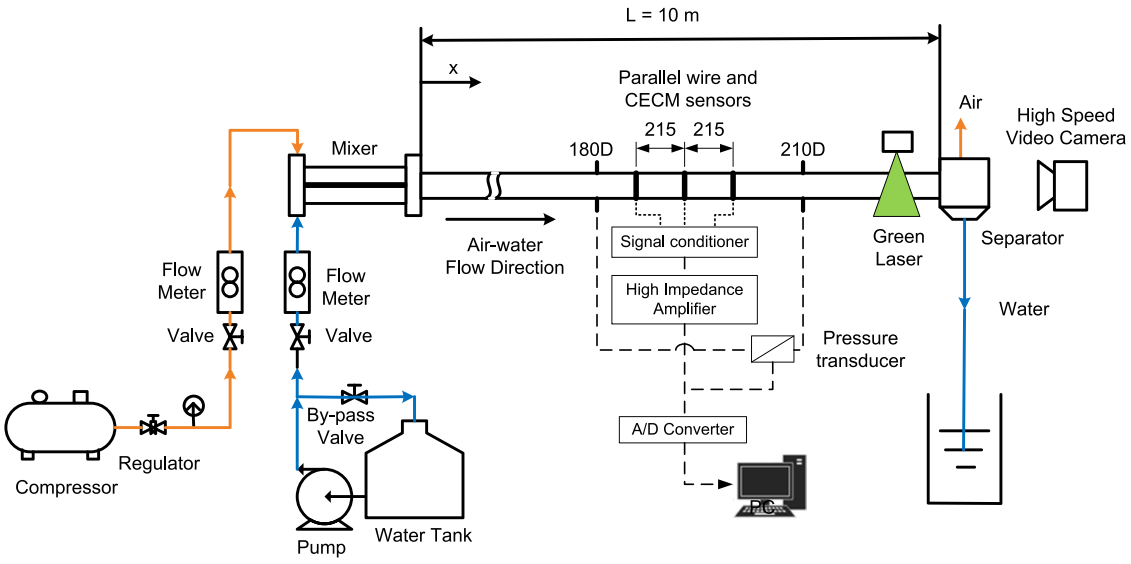

Fig. 1. Schematic diagram of the experimental apparatus.

$$\frac{1}{R_{TP}} = \frac{1-\eta}{R_G} + \frac{\eta}{R_L} \tag{1}$$

where R_G and R_L are the electrical resistance of the gas and liquid phases that have individually occupied the pipe section. Liquid hold-up (η) is the function of the two-phase voltage drop (V_{TP}) in the unit of pipe length when the electrical current I_0 is given. Hold-up is expressed by the following equation, noting that in two-phase flows of air-water, the value of $R_G \gg R_L$.

$$\eta = \frac{R_L}{R_{TP}} = \frac{I_0 R_L}{I_0 R_{TP}} = \frac{V_L}{V_{TP}} \tag{2}$$

where V_L is the voltage drop when the liquid has occupied a certain amount of area in the pipe.

Moreover, the visualization of the circumferential film thickness was also taken at the distance of 30D from upstream of the air and water separator as shown clearly in Fig. 4, where D is the diameter of the pipe. In order to support the flow visualization, the test section was also equipped with a green laser sheet to obtain axial view of the cross sectional area of the test pipe. Furthermore, the axial stratified flow phenomenon was captured by using a high speed video camera with a recording rate of 400–1200 fps, the image resolution of 1280 × 800, and a focal length of 85.

Fig. 5 shows the steps of the image processing of the video images obtained from the present work to validate the circumferential liquid film thickness data obtained from the parallel wire sensors. There were two steps in the cropping process: (1) circular cropping: to find the circumference, starting at the center. The area outside the circumference is marked by the black color, (2) square cropping: to find the correct area (shown in Fig. 6(a)). The next step was color image processing from RGB to gray scale (Fig. 6(b)) from the value of 0 (black) to 255 (white) or 256 Gy scale level. A median filter was applied to reduce the image noise. Then, the binary mode process (Fig. 6(c)) defined the transition boundary and finally, an object analysis (post-processing) to determine the wetted wall angle and flow parameters as shown in Fig. 6(d) was conducted.

To determine the interfacial shear stress between gas and liquid of stratified flow, the equations in separated two-fluid model should be solved. Hence the experimental data of the pressure gradient and the liquid hold-up are needed. For this reason, pressure gradient

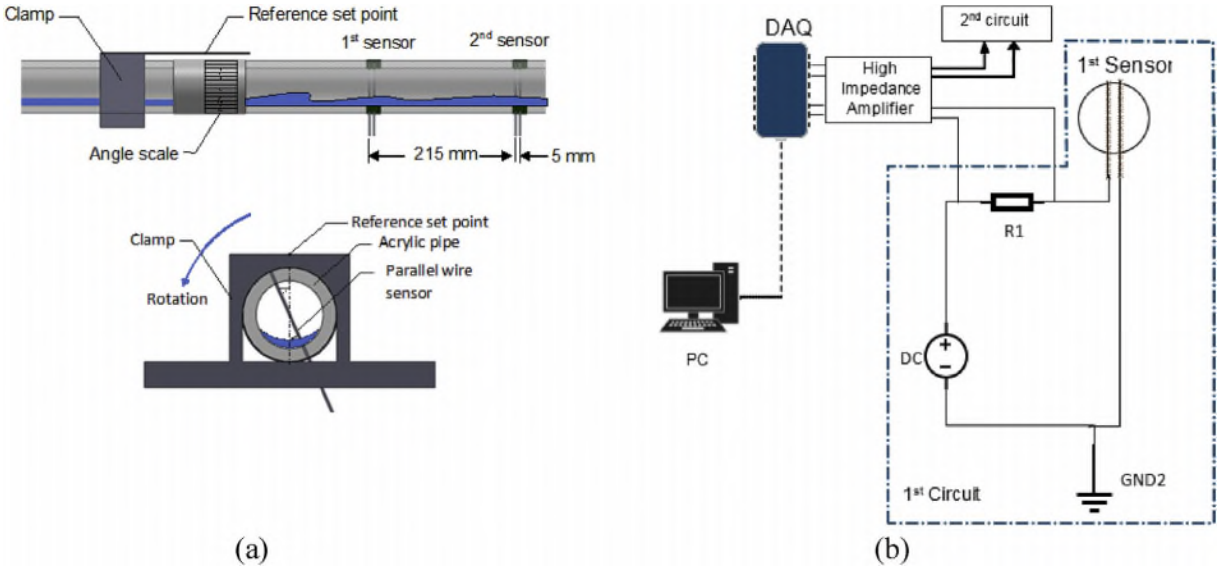

Fig. 2. (a) A parallel wire sensor at a tested pipe (b) A schematic diagram of the liquid film measurement.

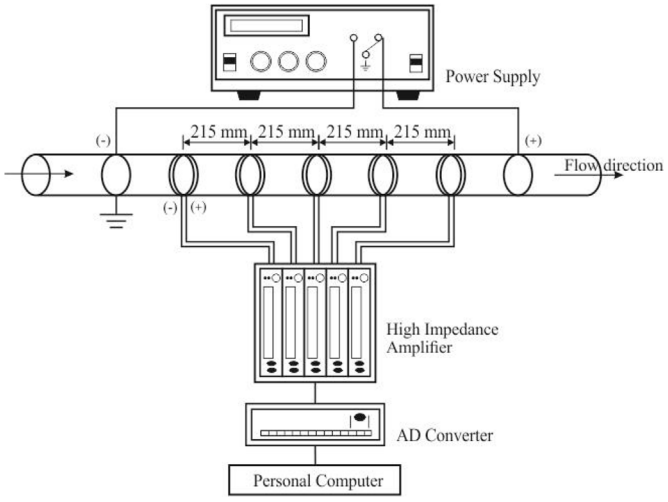

Fig. 3. The schematic diagram of the constant electric current method (CECM) to measure the instantaneous liquid hold-up used in the present work (Deendarlianto et al., 2019).

measurements $\left(\frac{dp}{dx}\right)$ between two locations were measured using the Validyne® pressure transducers. The uncertainty level of this transducer at full scale is 0.25%.

3. Results and discussions

3.1. Interfacial shape patterns

Fig. 7 shows the effect of J_G on the interfacial behavior and the change of liquid hold-up versus time for the gas-liquid stratified two-phase flow in a horizontal pipe under a constant of $J_L = 0.02$ m/s, thus representing the interfacial shape at low values of J_L. In Fig. 7(a), (i), (ii), (iii), and (iv) correspond to the cases of $J_G = 4$ m/s, $J_G = 8$ m/s, $J_G = 12$ m/s, and $J_G = 16$ m/s respectively. Close observation on the figures reveals that the J_G affects the interfacial shape inside the test pipe. At $J_G = 4$ m/s as shown in Fig. 7(a) (i), it is observed that the interfacial shape is flat, and becomes concave when the J_G becomes 8 m/s () (ii)). This means that the increase of the J_G tends to change the interfacial shape from a flat-shaped interface to a concave-shaped interface. This phenomenon is explained physically as follows. The increase of J_G produces a rough gas-liquid interface and a secondary gas recirculation, which is the local recirculation of gas before a wave ligament. It results in a higher interfacial shear stress, which becomes a significant driving force to sustain the liquid film rise on the upper side of the pipe wall as reported by Laurinat et al. (1985). Therefore, the interfacial shape changes from a flat-shaped interface to a concave-shaped interface. The obtained phenomenon also has a good agreement with that of Setyawan et al. (2017) who conducted experiments on the WWF mechanism during the transportation of gas-liquid annular two-phase flow at low J_L in horizontal pipes. There is also a visible decrease in the liquid hold-up (η) at the bottom part of the pipe with the increase of J_G as shown in Fig. 7(b). Moreover, the liquid droplets in the gas core can be seen clearly at $J_G = 16$ m/s () (iv)). This is due to the interfacial shear stress between the liquid and gas phases being large enough to disrupt the formed liquid ligament and produces liquid drops, therefore, the liquid droplet inside the gas core was able to be detected here.

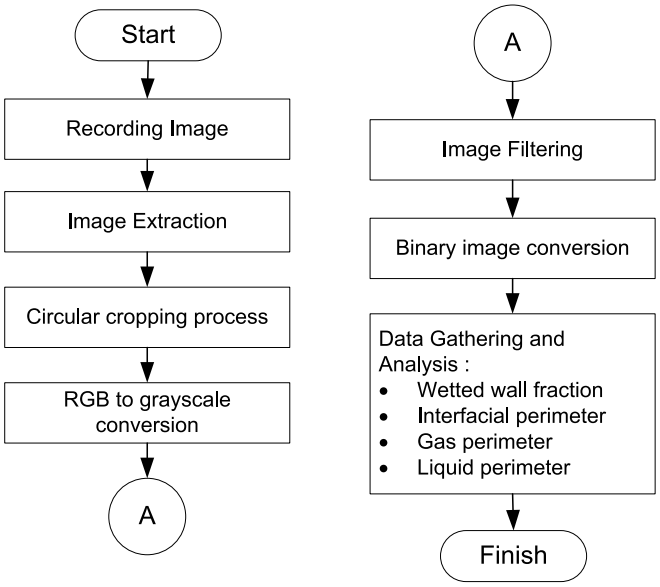

Fig. 5. The image processing steps of the video image data.

Fig. 8 shows the effect of J_G on the interfacial behavior of the gas-liquid stratified two-phase flow in a horizontal pipe under a constant $J_L = 0.075$ m/s, thus representing the interfacial shape at high values of J_L. In Fig. 8(a), (i), (ii), (iii), and (iv) correspond to the cases of $J_G = 4$ m/s, $J_G = 8$ m/s, $J_G = 12$ m/s, and $J_G = 16$ m/s respectively. In comparison to the interfacial behavior at low values of J_L as shown in Fig. 7, it is noticed that the interfacial shapes at high values of J_L change dramatically. Under the same $J_G = 4$ m/s as an example, the interfacial shape at $J_L = 0.075$ m/s is a concave as shown clearly in Fig. 8(a) (i), meanwhile, it has a flat-shaped interface at $J_L = 0.02$ m/s (Fig. 6(a) (i)). In addition, small drops were also detected in the gas core at high values of J_L, meanwhile they were not found at low values of J_L. Next, there is also a visible decrease in the liquid hold-up at the bottom part of the pipe with the increase of J_G. Moreover, the number of liquid

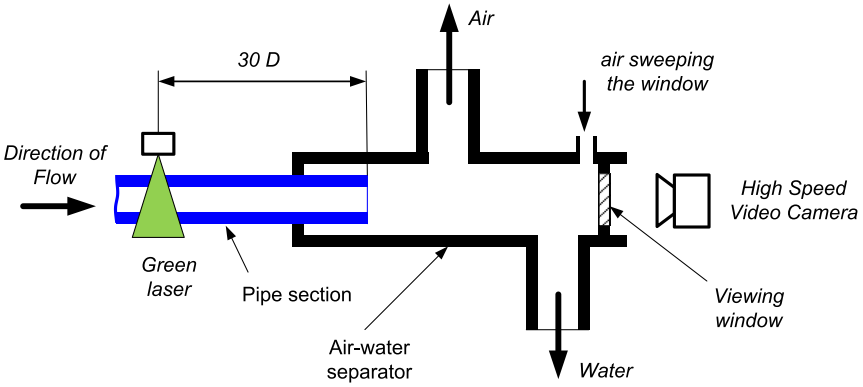

Fig. 4. Axial view of the gas-liquid separator.

Fig. 6. The example of image processing steps: a. Cropping image, b. Grayscale image, c. BW image, d. Wetted wall angle dan perimeter plotted at the original image.

droplets in the gas phase also increases with the increase of the J_G as indicated also by Badie et al. (2001) who carried out the observation of the axial viewing studies in a horizontal pipe of a co-current stratified two-phase flow. This can be explained that the increase of J_G will increase the interfacial shear stress between the liquid and gas phases. This stress will disrupt the formed liquid ligaments and produce liquid drops. Consequently, the production of liquid droplets inside the gas phase will increase too.

The interfaces of gas and liquid show a strong roughness with the increase of J_G. As apparent in the figures below, the size and the number of liquid droplets respectively decreased and increased with the increase of J_G. It can be seen by comparing) (ii), 8(a) (iii) and 8(a) (iv).

Fig. 9 shows the effect of J_L on the interfacial profile of a gas-liquid stratified two-phase flow in a horizontal pipe under a constant J_G = 4.0 m/s, thus representing the interfacial shape at low values of J_G. In Fig. 9(a), (i), (ii), and (iii) correspond to the cases of J_L = 0.02 m/s, J_L = 0.04 m/s, and J_L = 0.075 m/s, respectively. Under close observation of the figures, we notice that under a constant low value of J_G, the interfacial shape changes from a flat-shaped interface to a concave-shaped interface with the increase of the J_L. A concave-shaped interface is distinguished based on the combination of visual observation and data analysis of liquid film thicknesses as shown in the figures of circumferential liquid film thickness. In the range of experimental matrix under the same J_L, the concave-shaped interface started to appear at J_L = 0.075 m/s, where the entrainment of liquid droplets also exist in the gas core.

Fig. 10 shows the effect of J_L on the interfacial profile of gas-liquid stratified two-phase flow in a horizontal pipe under a constant J_G = 16.0 m/s, thus representing the interfacial shape at high values of J_G. In Fig. 10(a), (i), (ii), and (iii) correspond to the cases of J_L = 0.02 m/s, J_L = 0.04 m/s, and J_L = 0.075 m/s, respectively. The figures indicate that more dramatic changes are found when the J_G is high. That is, the interfacial shape is the concave-shaped interface, where the dispersed entrainments of liquid droplets in gas core are found. The interfaces of gas and liquid show a higher level of roughness with the increase of J_G. Also, the size and the number of liquid droplets decrease and increase with the increase of J_G respectively. It can be seen by comparing) (ii), and 10(a) (iii). Some of the liquid droplets stay on the pipe wall and deposit around the pipe wall to produce a concave shape interface of the stratified liquid film as reported by Anderson and Russell (1970) who conducted an experimental study on the film formation of a two-phase annular flow in a horizontal pipe. Furthermore, the increase of J_G will logically decrease the liquid film thickness or liquid hold-up, and will consequently decrease the surface tension in the liquid part. According

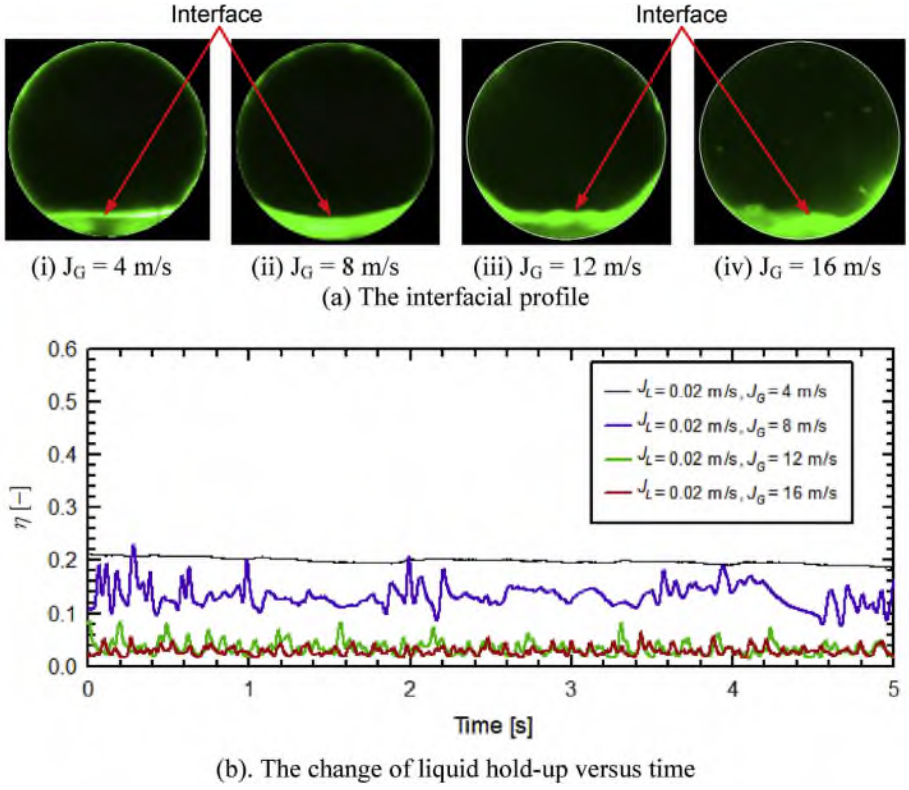

Fig. 7. The effect of J_G on the interfacial profile and the change of liquid hold-up versus time at low J_L of 0.02 m/s.

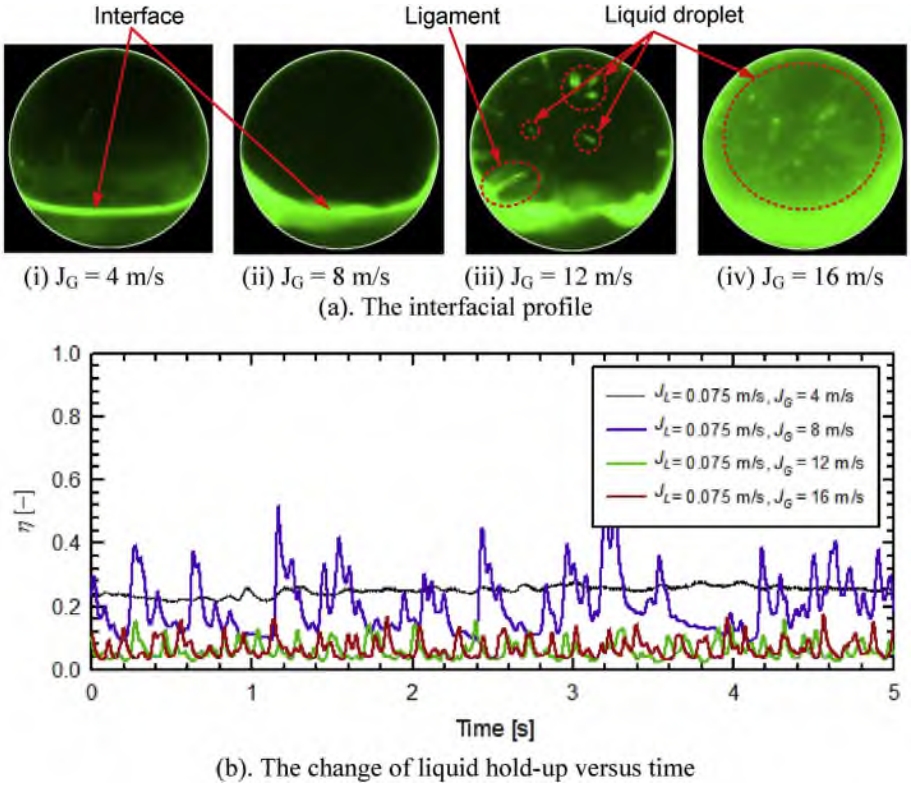

Fig. 8. The effect of J_G on the interfacial profile and the change of liquid hold-up versus time at high J_L of 0.075 m/s.

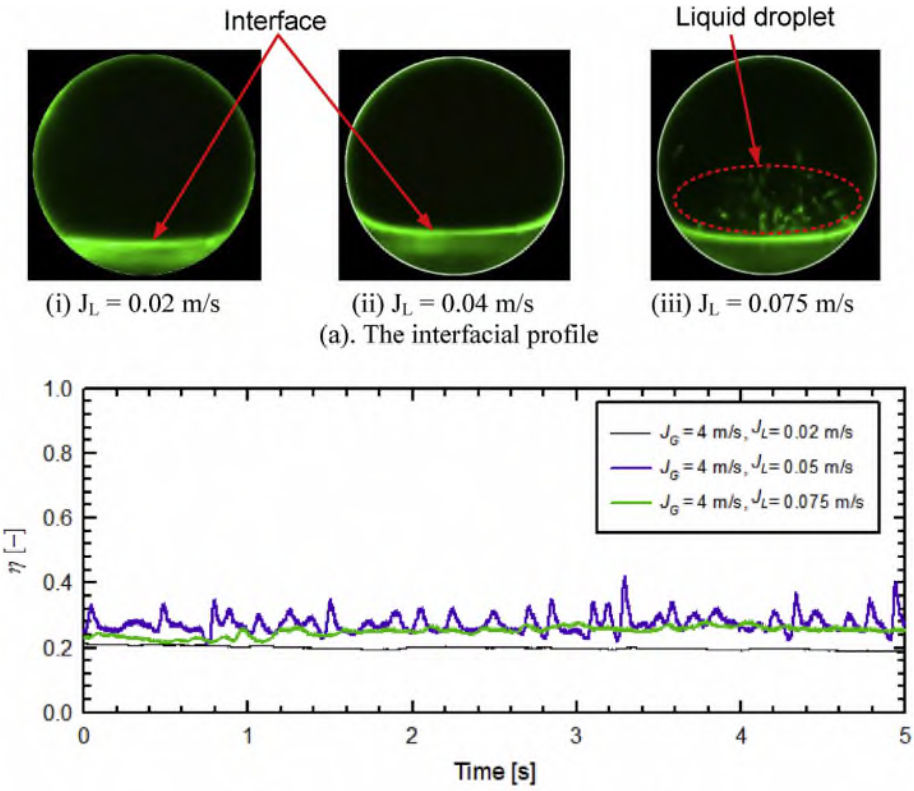

Fig. 9. The effect of J_L on the interfacial profile and the change of liquid hold-up versus time at low J_G of 4 m/s.

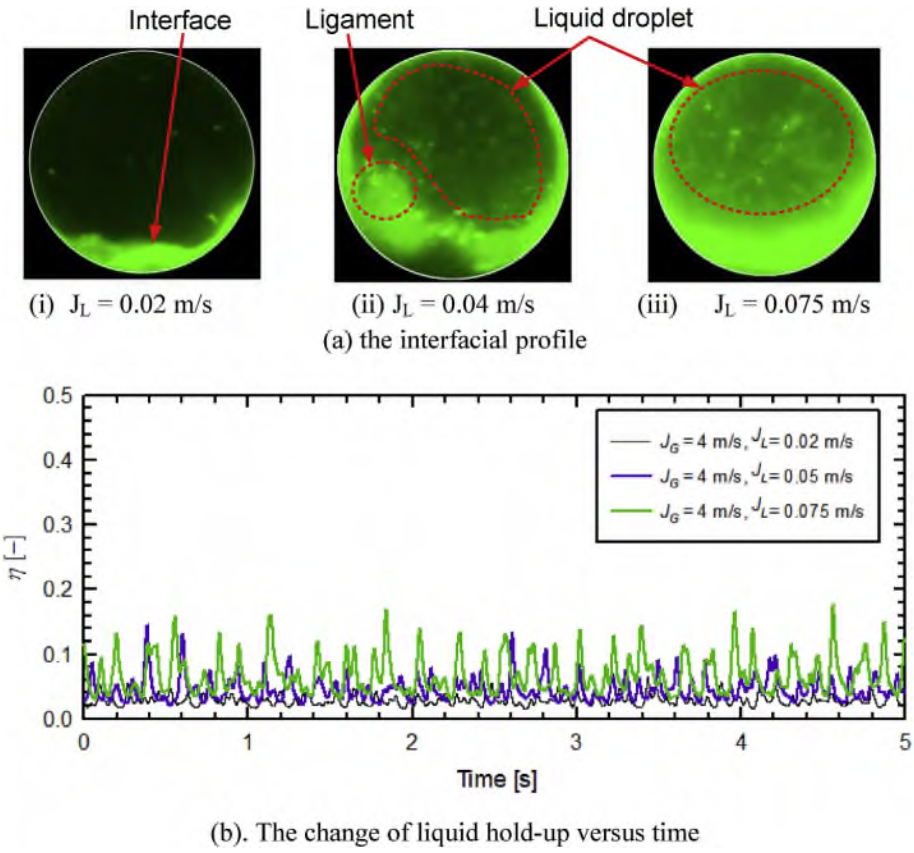

Fig. 10. The effect of J_L on the interfacial profile and the change of liquid hold-up versus time at high J_G of 16 m/s.

to physics, with every increase in ^{J}G, the area of the pipe occupied by gas will increase and hence reduce the area occupied by liquid. On the other hand, the increase of J_G results in a high interfacial shear stress and large amplitude of wavy flow that lead to the initiation of the liquid entrainment process, and produces the liquid ligament. This ligament is unstable, therefore, it stretches into the liquid filament that breaks up into smaller liquid droplets in the gas core.

3.2. Shape parameters

3.2.1. Circumferential liquid film thickness

To examine the validity of the visual observation study, the circumferential liquid film thickness measurement was carried out using developed parallel wire sensors. The results are shown in Figs. 11 and 12. Here the effects of J_L and J_G are depicted in Figs. 11 and 12, respectively. The figures show that the flow behavior obtained from the visual observations is similar to that of the measured circumferential liquid film thickness. That is, the increase of J_L under a constant J_G will change the interfacial shape from a flat-shaped interface into a concave-shape interface. As can be seen in Fig. 11, at the flow condition of J_L = 0.03 m/s and J_G = 5 m/s, it is noticed that the film thickness tends to produce a flat interface, meanwhile it will change into a concave-shaped interface when the superficial gas velocity increases from J_G = 5 m/s to 8 m/s. Next, the increase of J_G decreases the liquid film thickness and increases the perimeter of the wetted wall fraction in the pipe due to the increase of shear stress at the interface of the liquid film. Furthermore, the increase of the J_L affects the interfacial shape of the liquid film in the tested pipe. As shown in Fig. 12, it is noticed that under a constant J_G the liquid film thickness and perimeter of the wetted wall fraction increase with the increase of liquid velocity. It conforms to the results obtained from the visual observation described above and the experimental results from Fukano and Ousaka (1989) who conducted the liquid film measurements of gas-liquid annular

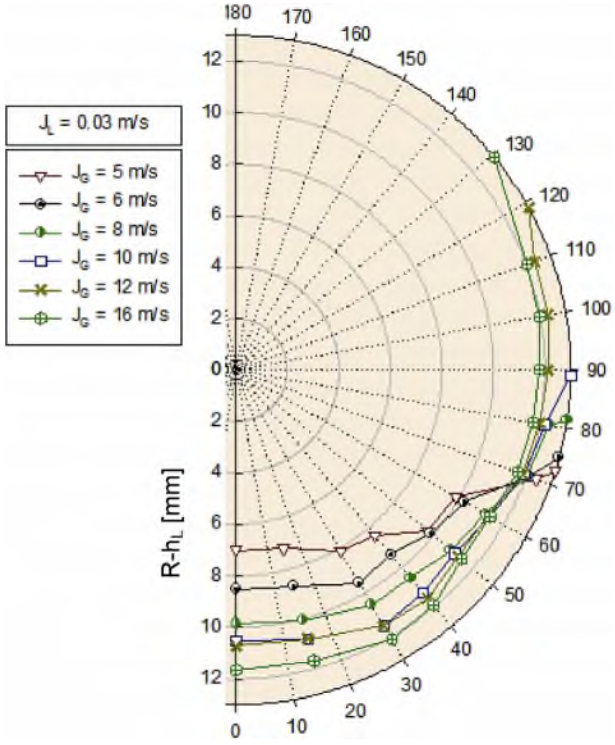

Fig. 11. The effect of J_G on the circumferential liquid film thickness under a constant J_L = 0.03 m/s.

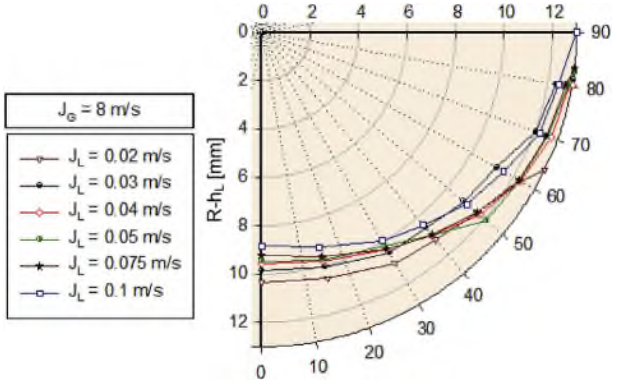

Fig. 12. The effect of J_L on the circumferential liquid film thickness under a constant J_G = 8.0 m/s.

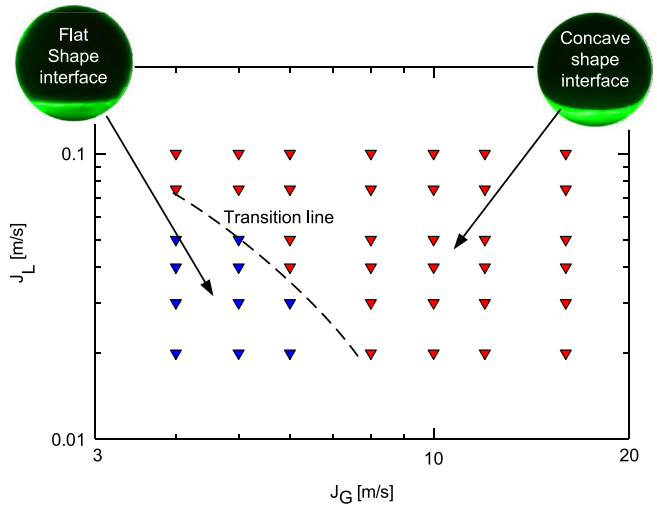

Fig. 13. The transition line of the interfacial shape.

flows in horizontal pipes.

Fig. 13 depicts the transition map of the WWF of the gas-liquid stratified flow in a horizontal pipe obtained from the present experimental study, which are plotted on a J_G and J_L map. This map was obtained by taking into account all the data including the video images, the time variation of the liquid hold-up, and the circumferential liquid film thickness as described above. In the map, a thick dashed line represents the boundary of the interfacial shape, and the solid symbols indicate the experimental points. Close observation of the figure reveals that the transition from a flat-shaped interface to a concave-shaped interface is affected by both J_L and J_G. The increase of J_L and J_G will change the interfacial shape from a flat-shaped interface into a concave-shaped interface. Note that the concave-shaped interface begins under the condition around J_G = 8 m/s.

3.2.2. Contact angle

Fig. 14 shows the effect of the relationship between J_G, J_L, and θ_1 obtained from the present experiment. Close investigation of the figure indicates that in the region of flat-shaped interfaces (at low J_G), the increase of J_G up to a certain extent (J_G < 8 m/s) will not affect the change in θ_1 when J_L is kept constant. This is due to the inertia of the gas not being strong enough to supress the fluid, thus causing θ_1 to not change significantly. However, when J_G is kept constant, θ_1 increases with the increase of J_L. The possible reason behind this is that the increase of J_L will increase the liquid hold up (η) or the liquid film thickness (h_L) and consequently increasing the interfacial perimeter length (S_i). As a result, θ_1 becomes larger.

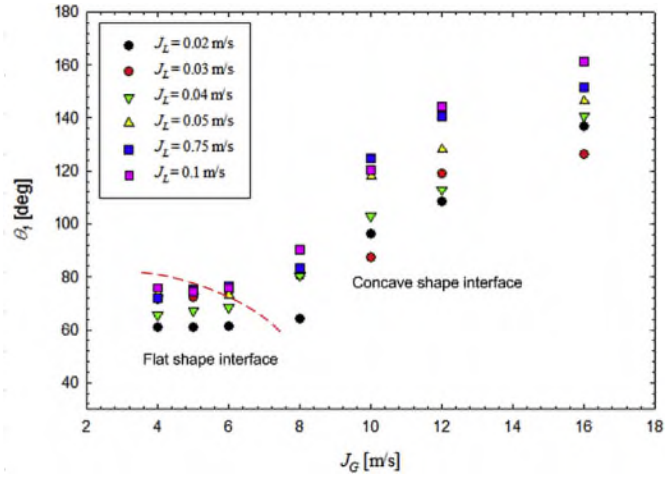

Fig. 14. The effects of J_L and J_G on the measured θ_1.

However, in the region of concave shape interface (J_G > 8 m/s), the θ_1 increases with the increase both of J_G and J_L. An increase in J_G will cause the inertia of the gas to increase, therefore the liquid will be pushed down and cause a portion of the liquid to climb up the pipe wall, showing an increase in θ_1. Another phenomenon that happens under higher values of J_G is the detachment of droplets that climbed up the pipe wall and forming a film. This will increase the θ_1 value as well. Furthermore, an increase of J_L will increase the liquid hold-up or the liquid film thickness in the test pipe. Therefore, the area occupied by the liquid also increases, hence, increasing the θ_1.

3.2.3. Interfacial perimeter

Interfacial perimeter is determined by using the concept of the double-circle model as introduced by Brauner et al. (1996) and Ahn et al. (2018). They proposed the model to describe a concave-shaped interface for stratified wavy flow while assuming that it is an imaginary eccentric circle as shown in Fig. 15(b). In Fig. 15(b), h_L is the liquid film thickness at the bottom part of the test pipe, R is the inner radius of the test pipe, S_i is the interface perimeter, θ_1 is the contact angle, R_2 is radius of thick broken line of outer circle, and Δ is the eccentricity of the center of both circles.

The points of (x_1, y_1), (x_2, y_2), and (x_3, y_3) were determined from the liquid film thickness measurement by using parallel wire sensors, and were validated by using the image analysis of the video image obtained from the present experimental study. Next R_2 and Δ can be calculated by using the basic equation of the circle. And is stated as follows:

$$x_1 = -R\sin\theta_1\ ;\ y_1 = (R - h_L) - R\cos\theta_1\ ;\ \text{for}\ \theta_1 \le \pi/2 \tag{3}$$

$$x_3 = R\sin\theta_1\ ;\ y_3 = (R - h_L) - R\cos\theta_1\ ;\ \text{for}\ \theta_1 \le \pi/2 \tag{4}$$

$$x_1 = -R\sin\theta_1\ ;\ y_1 = (R - h_L) + R\cos\theta_1\ ;\ \text{for}\ \theta_1 > \pi/2 \tag{5}$$

$$x_3 = R\sin\theta_1\ ;\ y_3 = (R - h_L) + R\cos\theta_1\ ;\ \text{for}\ \theta_1 > \pi/2 \tag{6}$$

where (θ_2 - π) is the contact angle of the eccentric imaginary circle, the radius of eccentric circle (R_2) can therefore be calculated as:

$$R_2 = -\frac{R\sin\theta}{\sin(\theta_2 - \pi)} = -\frac{R\sin\theta}{\sin\theta_2} \tag{7}$$

And the interfacial perimeter can be determined with the following equation:

$$S_i = -\frac{2R\sin\theta_1}{\sin 2}[\theta_2 - \pi] \tag{8}$$

Fig. 16 shows the relationship between J_G and J_L towards the interfacial perimeter using the double-circle model. This figure shows the same trends as Fig. 14, where an increase in J_G causes the interfacial

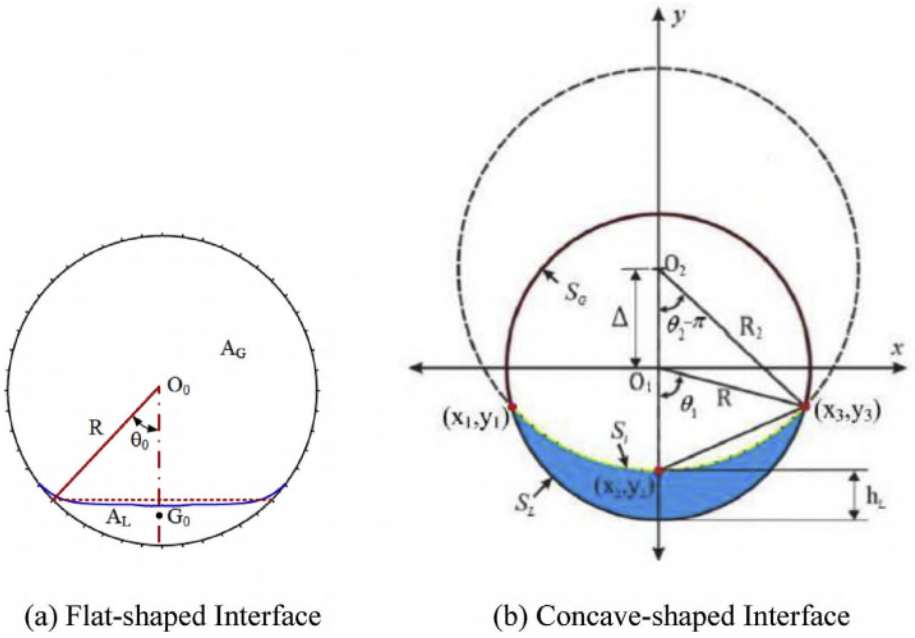

Fig. 15. Schematic geometries of (a) flat shape interface and (b) the double circle model of the concave shape interface of separated flow in a horizontal pipe.

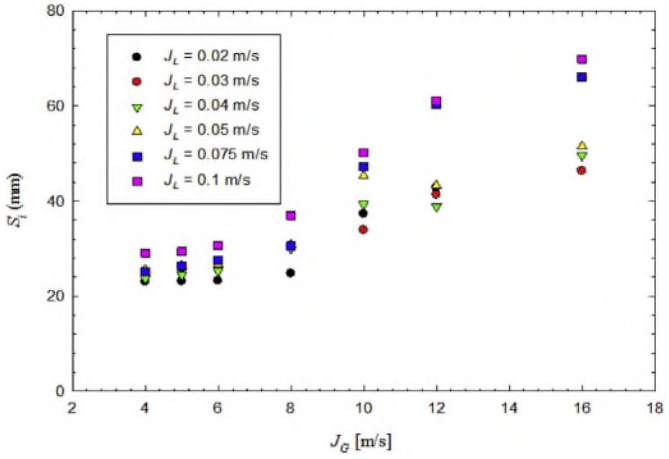

Fig. 16. The relationship between J_G and J_L on the interfacial perimeter.

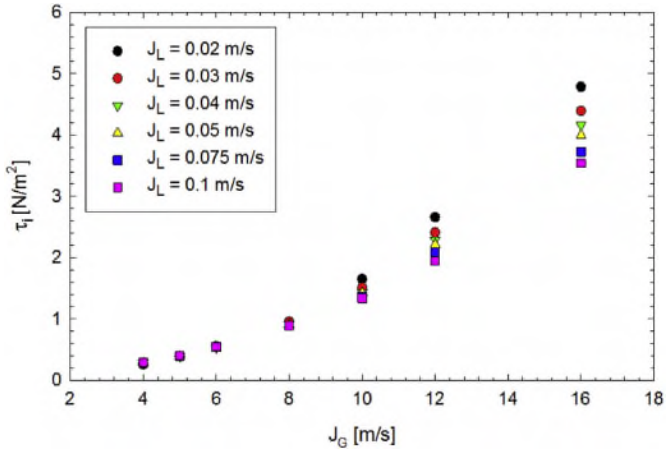

Fig. 17. The interfacial shear stress (τ_i).

perimeter to remain constant in area of flat-shaped interfaces and increase in the area of concave-shaped interfaces. Moreover, the increase of J_G will increase the interfacial shear stress between gas and liquid as shown in Fig. 17. In Fig. 17, the interfacial shear stress (τ_1) was calculated from the separated flow model, in which the pressure gradient (dp/dx) and the liquid hold-up were obtained from the measurements. The separated flow model which is based on solving two sets of equations governing the conservation of mass, momentum and energy is solved. For steady-state fully-developed gas-liquid flow in horizontal pipe with constant cross-sectional area, momentum balance of each phase are as follows:

$$-A_L\left(\frac{dp}{dx}\right) - \tau_{WG}S_L + \tau_i S_i = 0 \tag{9}$$

$$-A_G\left(\frac{dp}{dx}\right) - \tau_{WG}S_G - \tau_i S_i = 0 \tag{10}$$

Here it is noticed that the increase of τ_1 provokes the liquid film to move upwards according to the circumferential pipe wall. Consequently, it decreases the circumferential liquid film thickness and increases the S_i.

3.3. Semi analytical model development

From the viewpoint of engineering application, the concave-shaped interface is very important, therefore, a development of the experimental correlation to predict the contact angle to represent WWF is needed. In the next section, the development of this correlation will be given. It is developed to improve the accuracy of available correlations in open literature on the basis of real experimental data of concave-shaped interfaces. Here WWF is defined as the fraction of the pipe wall that is wetted by the liquid phase (denoted as Θ).

In the present work, a semi empirical correlation of the WWF in the region of the concave-shaped interface is developed on the basis of the energy balance in the liquid phase as indicated also by Hart et al. (1989). The basic concept of this energy states that the potential energy of the liquid phase (E_P) is the same as the product of the multiplication between the kinetic energy (E_K) of the same phase and its fraction (C) that contribute to climbing up the pipe wall. Here, it is postulated that the concave-shaped interface is formed due to the kinetic energy of the

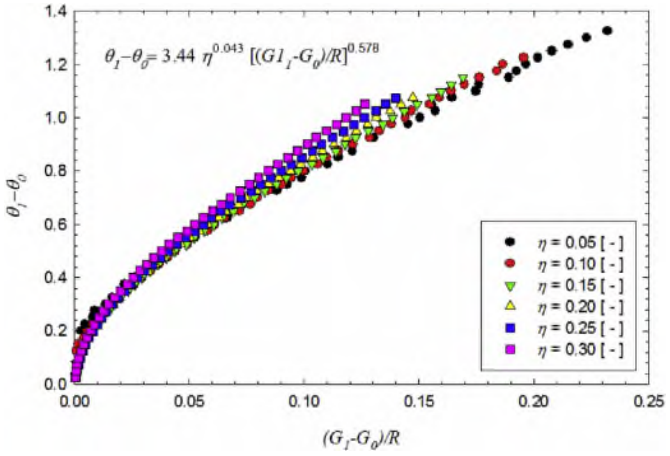

Fig. 18. The effect of $\frac{(G_1 - G_0)}{R}$ and liquid hold-up (η) on the ($\theta_1 - \theta_0$).

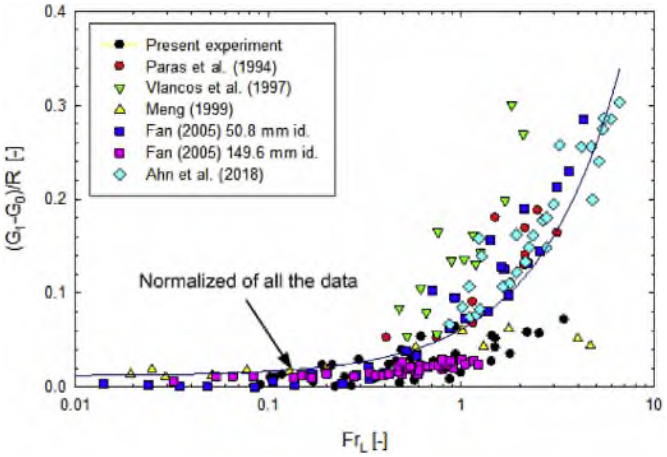

Fig. 19. The relationship between the $\frac{(G_1 - G_0)}{R}$ and Fr_L indicated in Eq. (6).

liquid phase propagating a portion of the liquid film to rise up the pipe wall. Moreover, E_P and E_K are defined as follows:

$$E_P = (\rho_L - \rho_G)\ \ (G_1 - G_0)\, g \tag{11}$$

$$E_K = \frac{1}{2}\,\rho_L U_L^2 \tag{12}$$

Where G_1 mentioned above is the distance of center of gravity of the gas phase under the condition of the concave-shaped interface with respect to the center of the pipe, meanwhile G_0 is the distance of the center of gravity of the liquid phase under the condition of the flat-shaped interface with respect to the center of the pipe. G_1 also corresponds to the minimum potential energy during the climb up of the liquid phase of the pipe wall. Next, ρ denotes the phase density, g denotes the acceleration of the gravity, and U denotes the actual velocity in the axial direction. The subscripts of L and G are the corresponding phases of liquid and gas respectively.

If Eq. (11) is substituted to Eq. (12), the geometrical and flow dynamic relationships are as follows:

$$\frac{(G_1 - G_0)}{R} = C\ Fr_L \tag{13}$$

Where Fr_L is the modified liquid Froude number, and is defined as

$$Fr_L = \frac{\rho_L}{(\rho_L - \rho_G)}\left(\frac{U_L^2}{g\ D}\right) \tag{14}$$

Fig. 18 shows the calculated result of the relationship between $\left[\frac{(G - G_0)}{R}\right]$ and (θ_1-θ_0), where the liquid hold-up (η) takes part as a parameter. The figure shows that the (θ_1-θ_0) increases with the increase of $\left[\frac{(G - G_0)}{R}\right]$, and is affected strongly byη. By using the statistical analysis, all the data can be correlated in the following equation.

$$(\theta_1 - \theta_0) = 3.44\,\eta^{0.043}\left[\left(\frac{G_1 - G_0}{R}\right)\right]^{0.578} \tag{15}$$

In Eq. (15), G_1 and G_0 and η were determined by using the proposed analytical solution from Brauner et al. (1996) at a given η as follows:

$$G_1 = \frac{R\ sin^3\theta}{\pi\ \eta\ sin^2\theta_2}(\text{cotan}\theta_2 - \text{cotan}\theta_1)\left[\pi - \theta_2 + \frac{1}{2}\sin(2\theta_2)\right] \tag{16}$$

$$G_0 = -\frac{2R\ sin^3\theta_0}{3\ \pi\ \eta} \tag{17}$$

$$\eta = \frac{1}{\pi}\left[\theta_0 - \frac{1}{2}\sin(2\theta_0)\right] \tag{18}$$

Next, Eq. (15) is normalized with π and results in the following relationship,

$$(\Theta_1 - \Theta_0) = 1.096\,\eta^{0.043}\left[\left(\frac{G_1 - G_0}{R}\right)\right]^{0.578} \tag{19}$$

The value of $\left(\frac{G_1 - G_0}{R}\right)$ can be substituted by the multiplication of the constant C and liquid Froude number (Fr_L) as indicated by Eq. (13) and the result is shown in Fig. 19, where [-] indicates that the units are dimensionless. In the figure, the data obtained from the present work are combined with those of the previous studies such as Paras et al. (1994), Vlanchos et al. (1998), Meng (1999), Fan (2005), and Ahn et al. (2018). The result indicates that all the data set are displayed closed together among each other, where the constant C is 0.05, which is obtained statistically from all the dataset. Therefore Eq. (19) can be written as follows:

$$(\Theta_1 - \Theta_0) = 1.096\,\eta^{0.043}(0.05\ Fr_L)^{0.578} \tag{20}$$

Equation (20) still leaves a crucial problem, where the Θ_0 is not defined yet. For this reason, a simple relationship between the θ_0 and η in a flat-shaped interface of gas-liquid stratified flow with low liquid loading ($\eta \leq 0.3$) can be developed from Eq. (17) as follow:

$$\theta_0 = 1.84\,\eta^{0.35} \tag{21}$$

If Eq. (21) is normalized with π, it results in the following relationship,

$$\Theta_0 = 0.858\,\eta^{0.35} \tag{22}$$

The substitution of Eq. (22) into Eq. (20) results the gives:

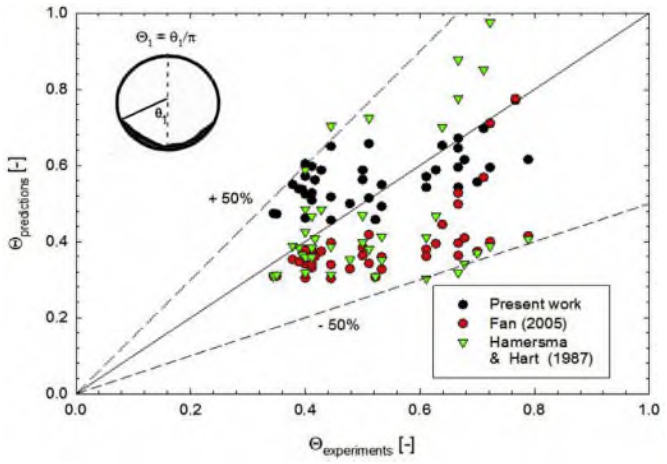

Fig. 20. The comparison of Eq. (23) with that of the obtained data from the present work, Fan (2005), and Hamersma and Hart (1987).

$$\Theta_1 = 0.86\,\eta^{0.35} + 1.096\,\eta^{0.043}(0.05\,Fr_L)^{0.578} \quad (23)$$

Where η is less than 0.30. To examine the performance of the developed equation, Eq. (15) is compared to the obtained experimental data from the present work, Fan (2005), and Hamersma and Hart (1987) as shown in Fig. 20. As seen in the figure, the correlation well-predicts the WWF data in the mean absolute percentage error (MAPE) of 20.6% within the error band of ± 50%.

4. Conclusion

The experimental study on the wetted wall fraction of gas-liquid stratified co-current two-phase flow in a horizontal pipe with low liquid loading was performed. The working fluids were air and water. The pipe length and inner pipe diameter were 10 m and 26 mm respectively. The superficial water (J_L) and air (J_G) velocities ranged from (0.02–0.075) m/s and (4–16) m/s respectively. The key finding can be noticed as follows:

1. From the analysis of the combination of the visual observation and the time average of circumferential film thickness, it is found that there are two kinds of interfacial shapes during the transportation of co-current gas-liquid stratified flows in a horizontal pipe. These are flat- and concave-shaped interfaces. These interfaces are strongly affected by both the J_L and J_G, where the increase of J_L tends to change the interface shape from a flat-into a concave-shaped interface. In the range of the examined J_L, the concave-shaped interface started at J_G = 8 m/s.
2. The WWF in the region of the concave-shaped interface, as indicated by the θ_1, increases with the increase both of J_L and J_G. However, in the region of the flat-shaped interface, the θ_1 is affected only by the J_L.
3. A semi empirical correlation to predict the wetted wall fraction (WWF) in the range of concave-shaped interface was developed. It can correlate the WWF data with the MAPE of 20.6%.

Acknowledgments

This present work was carried out within a research project funded by the Department of Mechanical and Industrial Engineering, Faculty of Engineering, Gadjah Mada University. The contract number was 817/H1.17/TMI/LK/2018. The authors would like to express their sincere appreciation for the high-speed video camera support from Chevron Indonesia.

List of symbols

A_G	Gas phase cross-sectional area
A_L	liquid phase cross-sectional area
C	Constant
dp/dx	pressure gradient
E_K	kinetic energy of the liquid phase
E_P	potential energy of the gas phase
Fr_L	liquid Froude number
G_0	liquid phase gravity center with a flat interface
G_1	gas phase gravity center with a concave interface
h_L	liquid film thickness
J_G	superficial gas velocity
J_L	superficial liquid velocity
R	radius of pipe
R_2	radius of the imaginary circle
S_i	interfacial perimeter
S_G	gas perimeter
S_L	Liquid perimeter
τ_i	interfacial shear stress
τ_G	gas shear stress
τ_L	liquid shear stress
U_L	liquid velocity
x,y	cartesian coordinates

Greek Letters

Δ	eccentricity of the center of both circles shown in Fig. 15
ρ_L	liquid phase density
ρ_G	gas phase density
θ_0	contact angle with a flat interface
θ_1	contact angle with a concave interface
θ_2	angle shown in Fig. 15
Θ_0	WWF with a flat interface
$\Theta 1$	WWF with a concave interface

Abbreviations

CECM	constant electric current method
MAPE	mean absolute prediction error
WWF	wetted wall fraction

Appendix A. Supplementary data

Supplementary data to this article can be found online at https://doi.org/10.1016/j.jngse.2019.102967.

References

Ahn, T., Moon, J., Bae, B., Jeong, J., Bae, B., Yun, B., 2018. An empirical model of the wetted wall fraction in separated flows of horizontal and inclined pipes. Chem. Eng. Sci. (178), 260–272.
Anderson, R.J., Russell, T.W.F., 1970. Film formation in two-phase annular flow. AIChE J. 16 (4), 626–633.
Ayati, A.A., Kolaas, J., Jensen, A., Johnson, G.W., 2014. A PIV investigation of stratified gas-liquid flow in a horizontal pipe. Int. J. Multiph. Flow (61), 129–143.
Badie, S., Lawrence, C.J., Hewitt, G.F., 2001. Axial viewing studies of horizontal gas-liquid flows with low liquid loading. Int. J. Multiph. Flow (27), 1259–1269.
Brauner, N., Rovinsky, J., Maron, D.M., 1996. Determination of the interface curvature in stratified two-phase system by energy consideration. Int. J. Multiph. Flow 22 (6), 1167–1185.
Deendarlianto, Rahmandhika, A., Widyatama, A., Dinaryanto, O., Widyaparaga, A., Indarto, 2019. Experimental study on the hydrodynamic behavior of gas-liquid air-water two-phase flow near the transition to slug flow in horizontal pipes. Int. J. Heat Mass Transf. (130), 187–203.
Dinaryanto, O., Prayitno, Y.A.K., Majid, A.I., Hudaya, A.Z., Nusirwan, Y.A., Widyaparaga, A., Indarto, Deendarlianto, 2017. Experimental investigation on the initiation and flow development of gas-liquid slug two-phase flow in a horizontal pipe. Exp. Therm. Fluid Sci. (81), 93–108.
Fan, Y., 2005. An Investigation of Low Liquid Loading Gas-Liquid Stratified Flow in Near-Horizontal Pipes. Ph.D. dissertation. The University of Tulsa.
Fukano, T., Ousaka, A., 1989. Prediction of the circumferential distribution of film thickness in horizontal and near-horizontal gas-liquid annular flows. Int. J. Multiph. Flow 15 (3), 403–419.
Fukano, T., 1998. Measurement of the time varying thickness of liquid film flowing with high speed gas flow by a constant electric current method (CECM). Nucl. Eng. Des. 184, 363–377.
Hamersma, P.J., Hart, J., 1987. A pressure drop correlation for gas/liquid pipe flow with a small liquid holdup. Chem. Eng. Sci. 42 (5), 1187–1196.
Hart, J., Hamersma, P.J., Fortuin, J.M.H., 1989. Correlations predicting frictional pressure drop and liquid hold-up during horizontal gas-liquid pipeflow with a small liquid hold-up. Int. J. Multiph. Flow 15 (6), 947–964.
Hudaya, A.Z., Widyatama, A., Dinaryanto, O., Juwana, W.E., Indarto, Deendarlianto, 2019. The liquid wave characteristics during the transportation of air-water stratified co-current two-phase flow in a horizontal pipe. Exp. Therm. Fluid Sci. 103, 304–317.
Laurinat, J.E., Hanratty, T.J., Jepson, W.P., 1985. Film thickness distribution for gas-liquid annular flow in a horizontal pipe. Phys. Chem. Hydrodyn. 6 (1/2), 179–185.
Meng, W., 1999. Low Liquid Gas-Liquid Two-phase Flow in Near-Horizontal Pipes. Ph.D. dissertation. The University of Tulsa.
Paras, S.V., Vlachos, N.A., Karabelas, A.J., 1994. Liquid layer characteristics in stratified-atomization flow. Int. J. Multiph. Flow 20 (5), 939–956.
Setyawan, A., Indarto, I., Deendarlianto, A., 2016. The effect of the fluid properties on the wave velocity and wave frequency of gas–liquid annular two-phase flow in a horizontal pipe. Exp. Therm. Fluid Sci. 71, 25–41.
Setyawan, A., Indarto, I., Deendarlianto, A., 2017. Experimental investigations of the circumferential liquid film distribution of air-water annular two-phase flow in a horizontal pipe. Exp. Therm. Fluid Sci. 85, 95–118.
Taitel, Y., Dukler, A.E., 1976. A model for predicting flow regime transitions in horizontal and near horizontal gas-liquid flow. AIChE J. 22 (1), 47–55.
Ullmann, A., Goldstein, A., Zamir, M., Brauner, N., 2004. Closure relations for the shear stresses in two-fluid models for laminar stratified flow. Int. J. Multiph. Flow 30 (7),

877–900.
Ullmann, A., Brauner, N., 2006. Closure relations for two-fluid models for two-phase stratified smooth and stratified wavy flows. Int. J. Multiph. Flow 32 (1), 82–105.
Vlanchos, N.A., Paras, S.V., Karabelas, A.J., 1998. Prediction of hold-up, axial pressure gradient and wall shear stress in wavy stratified and stratified/atomization gas/liquid flow. Int. J. Multiph. Flow (25), 365–376.
Vuong, D.H., Sarica, C., Pereyra, E., Al-Sharkhi, A., 2018. Liquid droplet entrainment in two-phase oil-gas low-liquid-loading flow in horizontal pipes at high pressure. Int. J. Multiph. Flow (99), 383–396.